Available online at www.sciencedirect.com
SCIENCE DIRECT®
Solar Energy 77 (2004) 803–814
SOLAR ENERGY
www.elsevier.com/locate/solener

High-efficiency polycrystalline CdTe thin-film solar cells

Xuanzhi Wu *

National Renewable Energy Laboratory (NREL), 1617 Cole Blvd., Golden C0 80401, USA

Received 12 December 2003; received in revised form 29 June 2004; accepted 30 June 2004
Available online 4 August 2004

Communicated by: Associate Editor T. M. Razykov

Abstract

Cadmium telluride is a promising photovoltaic material for thin-film solar cells. However, further improvements on performance and reproducibility of devices have been limited by the conventional SnO_2/poly-CdS/poly-CdTe device structure used for more than 30 years. In this paper, we review partial R&D approaches at NREL to understand the issues related to the conventional device structure and to develop several novel materials and a modified device structure for minimizing these issues. We have achieved a CdTe polycrystalline thin-film solar cell demonstrating an NREL-confirmed, total-area efficiency of 16.5% by using new materials and the modified device structure. To apply the high-efficiency CdTe cell fabrication technique, we developed two manufacturing processes for producing high-efficiency CdTe modules with the potential of high throughput and low cost.

Keywords: CdTe; Thin-film; High-efficiency

1. Introduction

Cadmium telluride (CdTe) has been recognized as a very promising material for thin-film solar cells. CdTe is a II–VI compound semiconductor with a direct optical bandgap of ~1.5 eV that is nearly optimally matched to the solar spectrum for photovoltaic (PV) energy conversion. CdTe also has a high absorption coefficient, $>5\times10^5$/cm, which means that ~99% of photons with energy greater than the bandgap (E_g) can be absorbed within 2 μm of CdTe film. Small-area CdTe cells with efficiencies of more than 15% have been developed (Britt and Ferekides, 1993; Ohyama et al., 1997). Large-area monolithic CdTe modules have also demonstrated high performance and the ability to attract production-scale capital investments (Ullal et al., 2000). However, further improvements on performance and reproducibility of CdTe cells have been limited by the conventional SnO_2/poly-CdS/poly-CdTe device structure used for more than 30 years (Adirovich et al., 1969). For example, conventional transparent conductive oxides, primarily SnO_2 films, have an average transmission of only 80% when a sheet resistivity of ~10 Ω/sq is used. This does not provide adequate design latitude when trying to optimize either device performance or manufacturing cost. The cadmium sulfide (CdS) window layer has a low bandgap (~2.4 eV) that causes absorption in the short-wavelength region. The CdS film with a thickness of 0.1 μm can absorb about 63% of the incident radiation with energy greater than E_g (Chu and Chu, 1993). Higher short-circuit current densities (J_{sc}) can be achieved by reducing the CdS thickness to improve the blue response

* Tel.: +1 303 3846552; fax: +1 303 3846430.
E-mail address: xuanzhi_wu@nrel.gov

0038-092X/$ - see front matter
doi:10.1016/j.solener.2004.06.006

in the conventional CdS/CdTe device structure. However, reducing the CdS thickness can adversely impact device open-circuit voltage (V_{oc}) and fill factor (FF) (McCandess and Hegedus, 1991). Finally, it is well known that the $CdCl_2$ treatment is important for making high-efficiency CdTe devices and offers several substantial benefits such as: increased grain size, grain-boundary passivation, increased CdS/CdTe interface alloying, and reduced lattice mismatch between the CdS and CdTe layers. However, one disadvantage of the $CdCl_2$ treatment is that over-treatment can result in loss of adhesion. The adhesion problems can limit the optimal $CdCl_2$ treatment process, as well as device performance.

In the past years, we tried to understand these issues related to the conventional device structure, and developed several novel materials and a modified device structure for minimizing these issues. We have developed the following: (1) a high-quality cadmium stannate (Cd_2SnO_4, or CTO) transparent conductive oxide (TCO) to replace the conventional SnO_2; (2) a high-resistivity $ZnSnO_x$ (ZTO) buffer layer located between the TCO and the CdS film; (3) an oxygenated, nanocrystalline CdS:O window layer with higher bandgap; (4) a modified CTO/ZTO/CdS/CdTe device structure; and (5) two manufacturing processes for producing high-efficiency CdTe modules, as an application of the high-efficiency CdTe cell fabrication technique.

In this paper, we review the preparation, properties, and application of new materials, the updated results of high-efficiency CdTe devices, and manufacturing processes.

2. Novel materials and their application in CdTe cells

2.1. Cadmium stannate transparent conductive oxide

CTO TCO films were prepared by RF magnetron sputtering. The deposition was carried out in pure oxygen at room temperature using a commercial hot-pressed oxide target. Then, CTO films were annealed at 600–660 °C in Ar or CdS/Ar atmospheres for 10–20 min. More details about the CTO film preparation have been described in previous papers (Wu et al., 1996a; Coutts et al., 1996).

CTO TCO films have several advantages over SnO_2 TCO films (Wu et al., 1996b; Wu et al., 1997). They have electrical resistivities ($\sim 1.5\times10^{-4}$ Ωcm) two times and six times lower than SnO_2 films produced using a $Sn(CH_3)_4$ (TMT) and $SnCl_4$ chemistry, respectively (see Table 1). Both SnO_2 films were prepared by chemical vapor deposition (CVD) at 400–500 °C, and doped with fluorine (F). The high conductivity of the CTO films is attributed to its high mobility with high carrier concentration. CTO films also have significantly better optical properties than conventional SnO_2 films. This is, in part, due to the lower resistivities, which allow thinner film to be used. Fig. 1 shows the transmittance and absorbance of the Cd_2SnO_4 and SnO_2 films with similar sheet resistivities (~10 Ω/sq). We can see from Fig. 1 that the CTO film has higher transmittance and lower absorbance than the SnO_2 film. It is worth noting that this feature can be maintained in the longer-wavelength region. Therefore, Cd_2SnO_4 films have the potential for application in polycrystalline thin-film multijunction devices (Wu et al., 2003a). In our earlier work, we pointed out that the excellent electrical and optical properties of Cd_2SnO_4 films are well-correlated to its single-phase spinel polycrystalline microstructure. Recently, we found that its high transmission and conductivity are

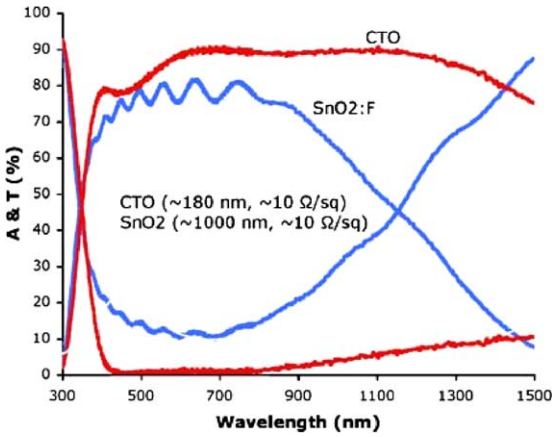

Fig. 1. Transmittance and absorbance of Cd_2SnO_4 and a SnO_2 films with similar sheet resistivity of ~10 Ω/sq.

Table 1
Comparison of electrical properties between Cd_2SnO_4 and SnO_2 films (Wu et al., 2000a)

Sample	Thickness (nm)	n (cm^{-3})	μ (cm^2/Vs)	Resistivity (Ωcm)	R_s (Ω/sq)
Cd_2SnO_4	510	8.94×10^{20}	54.5	1.28×10^{-4}	2.6
SnO_2 ($SnCl_4$)	~1000	4.95×10^{20}	15.4	8.18×10^{-4}	8.6
SnO_2 (TMT)	~1000	4.52×10^{20}	42.0	3.29×10^{-4}	3.3

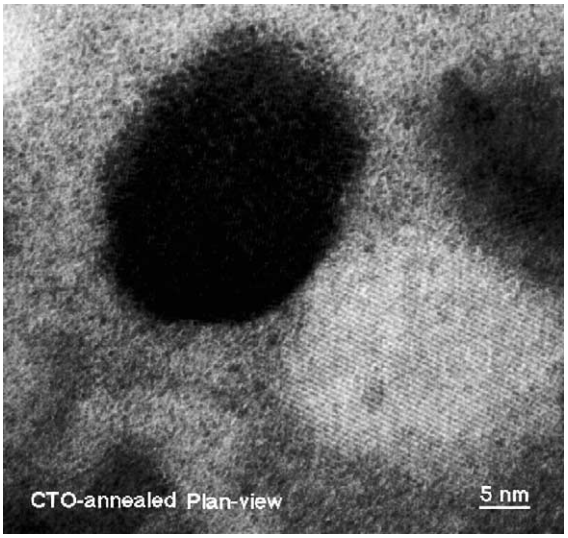

Fig. 2. TEM plan view of an annealed Cd_2SnO_4 TCO film (Wu et al., 2000a).

Table 2
J_{sc} loss due to TCO absorption for four different TCO films

TCO	R_s (Ω/sq)	J_{sc} loss due to TCO absorption (mA/cm^2)
SnO_2 ($SnCl_4$)	8–10	2.8
SnO_2 (TMT)	7–8	1.3
Cd_2SnO_4	7–8	0.62
CTO/ZTO	7–8/$\sim10^5$–10^6	0.68

related to its excellent microstructure and near-homogeneity (Wu et al., 2003a). Fig. 2 shows a transmission electron microscopy (TEM) plan view of an annealed CTO film. The extent of the fringes indicates that there is a high degree of material perfection. In contrast, there are a number of defects (such as dislocations and twins) in a typical SnO_2 film.

Because of the excellent material properties of Cd_2SnO_4 films, our results have demonstrated that J_{sc} can be improved by replacing the SnO_2 film with a CTO TCO film in CdTe cells. Table 2 shows the J_{sc} loss due to glass/TCO absorption for three different TCO substrates. We can calculate the J_{sc} loss due to glass/TCO absorption from their absorbance curves and AM1.5 solar spectrum in the CdTe active range between 300 and 860 nm. Three films were prepared on 7059 Corning glass (1.1–1.2 mm thick) and had nearly the same sheet resistivity. The CTO TCO has the lowest J_{sc} loss (0.7 mA/cm^2) due to its absorption in CdTe cells—two to four times lower than SnO_2 films prepared by the precursors TMT and $SnCl_4$, respectively.

2.2. High-resistivity zinc-tin-oxide buffer layer

In our earlier work, we used zinc stannate (Zn_2SnO_4) film as a buffer layer (Wu et al., 1998). In the preparation recipe of the Zn_2SnO_4 target, there is a high-temperature pre-reaction process that results in a problem in reproducibility. To simplify target preparation, we developed a $ZnSnO_x$ (ZTO) buffer layer to replace the Zn_2SnO_4 film. Both Zn_2SnO_4 film and $ZnSnO_x$ film have similar material properties, such as bandgaps of ~3.6 eV and resistivities of 1–10 Ωcm after post-anneal. ZTO films were prepared by RF magnetron sputtering. The deposition was performed in pure oxygen at room temperature using the commercial oxide target.

An as-grown ZTO film has a very high resistivity (>10^4 Ωcm). After post-anneal at higher temperature (540–620 °C) for 3–5 min, the film resistivity is reduced to 1–10 Ωcm. After anneal, the ZTO bandgap remains the same (~3.6 eV), but its transmission is slightly improved. By integrating a ZTO buffer layer in a CdTe cell, the probability of forming localized TCO/CdTe junctions can be significantly reduced when the CdS film is thinned, because the ZTO film has both high optical bandgap and high resistivity that roughly matches that of the CdS film. The ZTO buffer layer can also act as an "etch-stop" layer during the back-contact formation process and greatly reduce shunting problems (Wu et al., 2001a), because the ZTO film resists the etchant (e.g., a nitric/phosphoric-based, or NP, acid etchant) used for back-contact formation. For example, there is almost no etch for ZTO film in the NP etchant for more than 30 min, but ~1000-Å-thick chemical-bath-deposited (CBD) CdS film can be completely etched in the NP etchant within 20 min.

We also found that there is interdiffusion between the CdS and ZTO films. This interdiffusion can occur either at higher temperature (570–650 °C) in Ar, or at lower temperature (400–420 °C) in a $CdCl_2$ atmosphere (Wu et al., 2001b).

2.2.1. Interdiffusion at high temperature

In this study, two test samples were prepared. A CdS film and a ZTO film were deposited on independent 7059 Corning glass substrates by the CBD technique and RF magnetron sputtering, respectively. X-ray photoemission spectroscopy (XPS) was used to measure the changes of film composition before and after these films were annealed face to face at ~600 °C.

Fig. 3(a) indicates an absence of Cd in the ZTO film before annealing within the detection limits of XPS, and about 3–5 at.% Cd diffuses into the ZTO film from the CdS layer after annealing. Similarly, we cannot detect any Zn in the CdS film before annealing, whereas we detect about 2–3 at.% Zn in the CdS film after annealing (Fig. 3(b)).

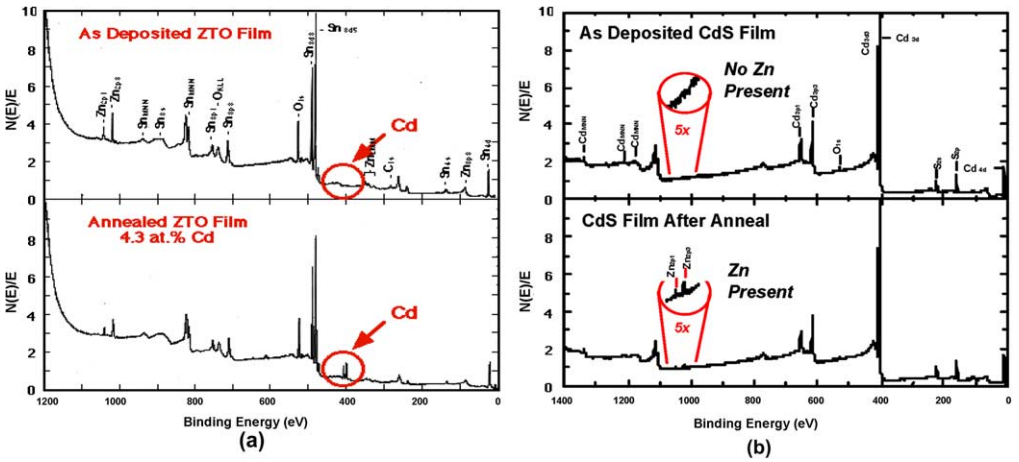

Fig. 3. XPS survey spectra of ZTO film (a) and CdS film (b) before and after annealing at ~600 °C in Ar (Wu et al., 2001b).

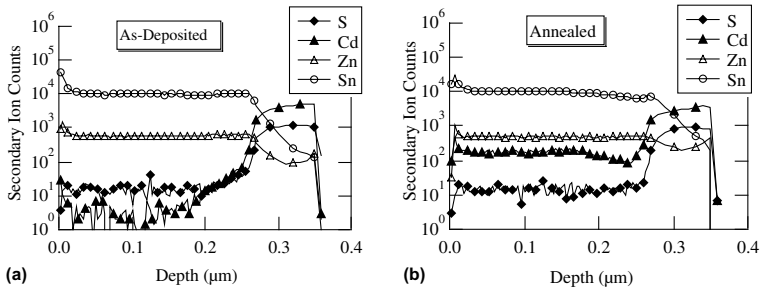

Fig. 4. Interdiffusion of ZTO and CdS films at 420 °C in a $CdCl_2$ atmosphere (SIMS data) (Wu et al., 2001b).

2.2.2. Interdiffusion at lower temperature in $CdCl_2$ atmosphere

A test sample with ZTO/CdS/glass structure was prepared and annealed at 420 °C for 15 min in a $CdCl_2$ atmosphere. Secondary-ion mass spectroscopy (SIMS) depth profiling was used to determine the extent of interdiffusion at the ZTO/CdS interface. SIMS data (see Fig. 4) also indicate a considerable amount of Cd and Zn diffusion into the ZTO and the CdS film, respectively.

In the later studies of TEM and energy-dispersive spectroscopy (EDS), we also found interdiffusion between the $ZnSnO_x$ and CdS films in a completed CdTe cell, in which the CdTe film was deposited at lower temperature (~570 °C) (Wu and Zhou, 2004).

We have successfully applied the interdiffusion feature to minimize issues related to the conventional SnO_2/CdS/CdTe device structure and to improve device performance and reproducibility. The interdiffusion of the CdS and ZTO layers improved the quantum efficiency of a CdTe cell over the entire active wavelength region (400–860 nm).

The interdiffusion "consumes" CdS film from both the CdTe and ZTO sides, rather than from one side (CdTe) in the conventional CdTe cell during device fabrication processes. Using this feature, we can improve the blue response of the device. This property may also be exploited in production by using thicker CdS films, thereby enhancing yield without reducing J_{sc}.

In the interdiffusion of the CdS and ZTO films, the ZTO film acts as a Zn source to alloy with the CdS film and form a $Zn_xCd_{1-x}S$ layer that has a higher bandgap than CdS. This shifts the short-wavelength cut-off to a smaller value (from ~520 to ~480 nm), which leads to an increase in J_{sc}.

The interdiffusion also significantly improves the adhesion between the TCO and the CdS layer after $CdCl_2$ treatment. Performance and reproducibility of CdTe cells are significantly influenced by the $CdCl_2$ treatment, which is used by all cell manufactures. However, a $CdCl_2$ over-treatment can result in adhesion-loss problems. Grain growth of the CdS film, which occurs during the $CdCl_2$ treatment, may introduce stress at the TCO/CdS interface, resulting in film blistering or peeling. The interdiffusion between the CdS and ZTO layers may relieve the stress at the CdS/ZTO interface, thereby improving device adhesion.

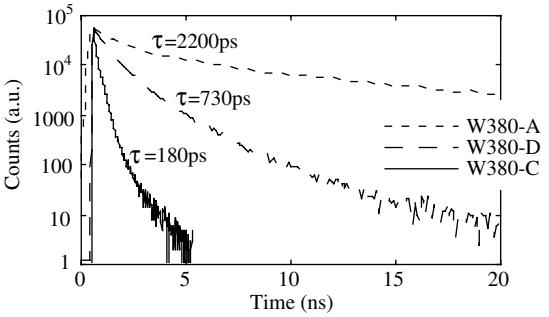

Fig. 5. TRPL decay curves of three CdTe cells with different $CdCl_2$ treatment (Wu et al., 2001b).

The significant improvement of device adhesion not only improves the device reproducibility, but also provides greater latitude in optimizing the $CdCl_2$ treatment process. Fig. 5 shows time-resolved photoluminescence (TRPL) results of three cells with different $CdCl_2$ treatment. We can see that an optimally $CdCl_2$-treated device (W380-A) has the longest TRPL lifetime (2.2 ns), which is three times higher than the device (W380-D) with a normal $CdCl_2$ treatment, and more than 10 times than the device (W380-C) without $CdCl_2$ treatment. NREL experimental results demonstrated that the TRPL lifetime correlates well with the quality of the junction and CdTe film, and with the absolute internal quantum efficiency in the wavelength region of 580–840 nm. For example, the 16.5%-efficient world-record CdTe cell (see Section 3) has TRPL lifetime of more than 2 ns, and also has an excellent red spectra response (see Fig. 11(b)). Even in CdTe cells prepared at lower temperature (~450 °C), there is still a direct correlation between TRPL lifetime and cell-efficiency parameters (Moutinho et al., 2000).

Finally, we found that the CdTe cell with a high-resistivity ZTO buffer layer has the lowest series resistivity of ~1 Ωcm^2. The mechanism related to improving device series resistivity is not yet completely clear, but we believe it is related to the interdiffusion feature and improvement of junction quality.

2.3. Oxygenated nanocrystalline cadmium sulfide window layer

In the conventional CdTe device, the poly-CdS film has been used most commonly as a window material. But it has three main issues that limit device performance. First, the $CdS_{1-y}Te_y$ alloy with lower bandgap can be formed between the CdTe and poly-CdS films, which affects device performance (McCandess and Hegedus, 1991). Second, poly-CdS film has a bandgap of ~2.42 eV, which causes considerable absorption in the short-wavelength region. Third, there is a nearly 10% lattice mismatch between the poly-CdTe film and the poly-CdS film, which causes high defect density at the junction region. To reduce the lattice mismatch between the CdS and CdTe films, high-temperature device fabrication processes must be used to enhance the interdiffusion of the CdS and CdTe films and form intermixed layers ($CdS_{1-y}Te_y$ and $CdTe_{1-x}S_x$). But during the high-temperature processes, new defects and impurities are introduced that limit the improvement of device V_{oc} and FF. Therefore, a new window material that has higher optical bandgap, a better lattice match with the CdTe absorber, and minimum Te diffusion is an important project for further improving CdTe cell performance.

We developed a novel window material, oxygenated nanocrystalline CdS film (nano-CdS:O), prepared at room temperature in an oxygen/argon gas mixture by RF magnetron sputtering. Details about the CdS:O film preparation have been described in previous papers (Wu et al., 2002; Wu et al., 2003b).

The CdS:O film has a higher optical bandgap (2.5–3.1 eV) than the poly-CdS film and has a nanostructure; the bandgap increases with an increase of oxygen content (from ~4 to ~23 at.% measured by XPS) and the grain size decreases (from about a few hundred angstrom to a

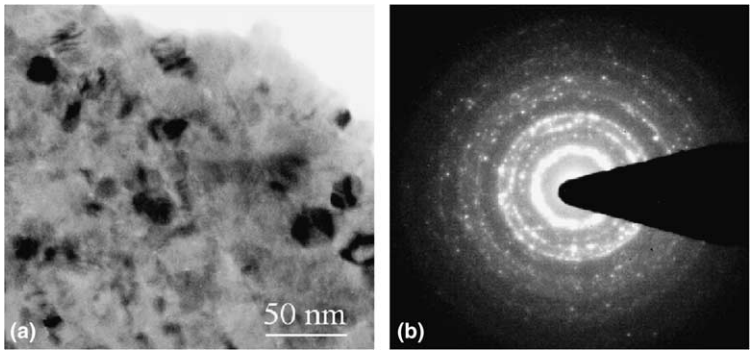

Fig. 6. TEM and electron diffraction pattern of CdS film deposited in pure Ar (Wu et al., 2003b).

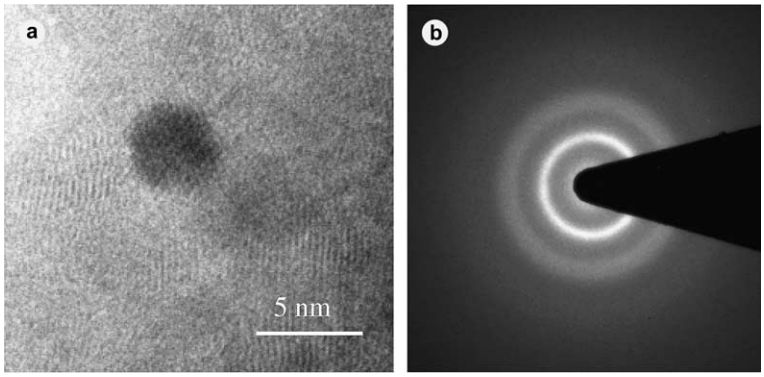

Fig. 7. TEM and electron diffraction pattern of CdS film deposited in 2% O_2/Ar gas mixture (Wu et al., 2003b).

few tenths angstrom measured by TEM). Fig. 6(a) shows a bright-field image of a CdS film sputtered in an oxygen-free environment. The average grain size is around 25 nm, which is consistent with the results from AFM. Fig. 6(b) shows a selected-area electron diffraction pattern taken from the same sample. It clearly reveals that the CdS film is polycrystalline. Fig. 7(a) shows a high-resolution TEM image of a CdS thin film sputtered in an 2% oxygen/argon environment. The film is still polycrystalline, but average grain size is around 3–5 nm, much smaller than the CdS film sputtered in an oxygen-free environment. Fig. 7(b) is a selected-area electron diffraction pattern, which was taken using the same select aperture as for Fig. 6(b). It shows diffraction rings only with no diffraction spots, indicating that the grain sizes are very small. Our TEM results suggest that one of the effects of oxygen in the growth environment is to reduce significantly the grain sizes of the sputtered CdS thin films, which results in the increase of their optical bandgap.

TEM and EDS results have also demonstrated that the higher oxygen content presented in the nanocrystalline CdS:O films can significantly suppress the Te diffusion from the CdTe into the CdS film and the formation of a $CdS_{1-y}Te_y$ alloy with a lower bandgap that results in poor quantum efficiency in the short-wavelength

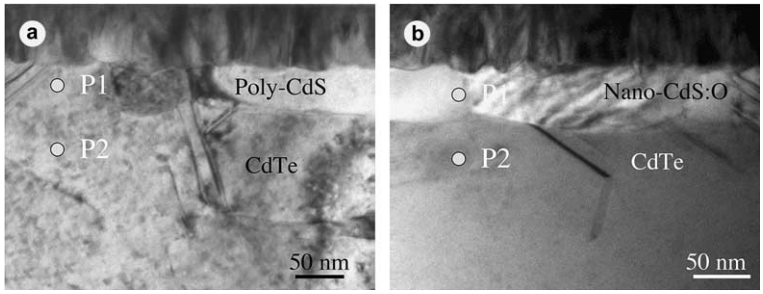

Fig. 8. Cross-sectional TEM images of a poly-CdS/CdTe cell (a) and a nano-CdS:O/CdTe cell (b) (Wu et al., 2003b).

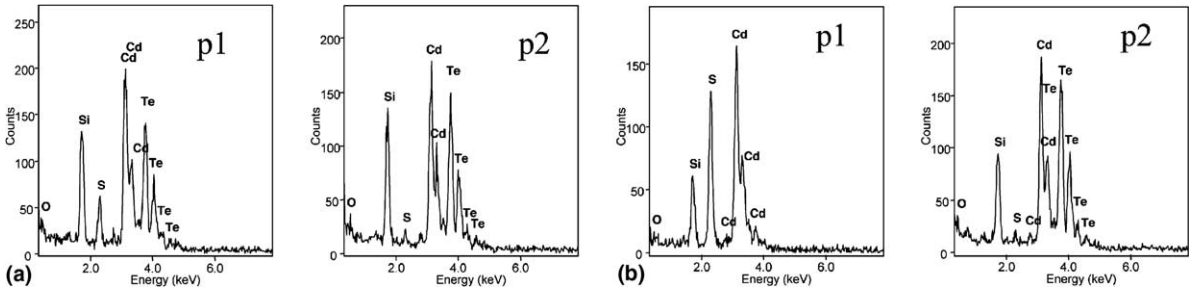

Fig. 9. EDS (a) (left) and (b) (right) taken from points P1 and P2 marked on Fig. 8(a) and (b) (Wu et al., 2003b).

region. Fig. 8(a) and (b) show cross-sectional TEM images of a poly-CdS/CdTe cell (a) and a nanocrystalline CdS:O/CdTe cell (b), respectively. In the poly-CdTe cell, the CdS film with a polycrystalline structure was deposited in pure Ar by RF sputtering. In Fig. 8(a), the CdS layer is not visible in some regions, which indicates total consumption of the CdS film. In some areas, the CdS is seen, but with significantly reduced thickness, suggesting that the CdS consumption is spatially variable in the plane of the film. The EDS measurements (see Fig. 9(a)) also indicate Te diffusion into the CdS layer (point P1 in Fig. 8(a)). Optical bowing in the $CdS_{1-y}Te_y$ alloy system is such that small changes in the Te content of CdS can result in a large decrease in bandgap (Ohata et al., 1973; Wei et al., 2000). The formation of $CdS_{1-y}Te_y$ alloy having a lower bandgap results in poor quantum efficiency in the short-wavelength region. In contrast, the nanocrystalline CdS:O layer is still very visible (see Fig. 8(b)). The nanocrystalline CdS:O film has much higher oxygen atomic concentration than poly-CdS film (Wu et al., 2002). Therefore, this strongly indicates that oxygen present in nanocrystalline CdS:O films significantly suppresses the Te interdiffusion from the CdTe to the CdS film and the formation of a $CdS_{1-y}Te_y$ alloy. The EDS results (see Fig. 9(b)) also confirm that Te cannot be found in the CdS:O layer (point P1 in Fig. 8(b)), which results in a higher quantum efficiency in the short-wavelength region and a higher J_{sc}. The J_{sc} values up to near 26 mA/cm^2 in a CTO/ZTO/CdS:O/CdTe cell are achieved by using the nanocrystalline CdS:O film. The Si peak in Fig. 9(a) and (b) is due to contamination during preparation of the test sample.

3. CTO/ZTO/CdS/CdTe device structure and updated high-efficiency CdTe cell results

Fig. 10 shows the modified CTO/ZTO/CdS/CdTe device structure. In this device structure, a CTO TCO film deposited on a borosilicate glass replaces the conventional SnO_2 TCO film as a front contact, and a ZTO film is integrated as a buffer layer located between the CTO and CdS layers. The thickness of both CTO and ZTO films was varied from 100 to 300 nm. In this case, the CdS film was prepared by a CBD technique (Chu et al., 1992), using cadmium acetate [$Cd(C_2H_3O_2)_2$], ammonium acetate ($NH_4C_2H_3O_2$), ammonia hydroxide (NH_4OH), and thiourea [$CS(NH_2)_2$] in an aqueous solution. Integrating nanocrystalline CdS:O film into devices for preparing high-efficiency CdTe cells is under way, but it has been used in novel manufacturing processes (see Section 4). The CdTe films were prepared by the close-spaced sublimation (CSS) technique at 600–625 °C for 3–5 min in O_2/He atmosphere. After CdTe deposition, samples received a vapor $CdCl_2$ treatment at 400–430 °C for 10–15 min. HgTe:CuTe-doped graphite paste annealed at ~270 °C for 30 min, followed by a layer of Ag paste, was then applied to the devices as the back-contact layer. An ~1000 Å MgF_2 antireflection (AR) coating was deposited on some of the cells.

Using the modified CTO/ZTO/CdS/CdTe device structure, we achieved a high FF of 77.34%, a high J_{sc} of near 26 mA/cm^2, and an efficiency of 16.5% measured by NREL's standard current–voltage (I–V) measurement, which represents individual optimized cases. NREL's standard I–V test conditions are 1000 W/m^2 illumination intensity under AM1.5 global solar spectrum, and cell temperature of 25 °C.

3.1. High fill factor

Table 3 lists I–V parameters of two high-efficiency CdTe cells with FF of more than 77%. These are the highest FF values ever reported for CdS/CdTe polycrystalline thin-film solar cells. Device analyses indicate that these cells with a high FF have a lower series resistivity R_s (~1 Ωcm^2), a higher shunt resistivity R_{sh} ($3–5 \times 10^3$ Ωcm^2), and better diode quality factor A (1.6–2). The reduction of R_s is mainly due to the use of a CTO

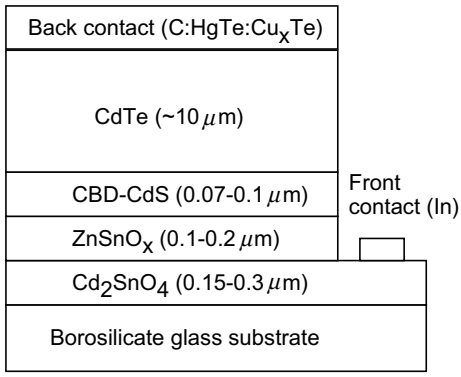

Fig. 10. Modified CTO/ZTO/CdS/CdTe device structure.

Table 3
High-efficiency CdTe cells with high fill factor (Wu et al., 2001a)

Cell #	V_{oc} (mV)	J_{sc} (mA/cm^2)	FF (%)	Efficiency (%)	Area (cm^2)
1	842.1	24.12	77.26	15.7	1.001
2	848.1	23.97	77.34	15.7	0.976

Table 4
High-efficiency CdTe cells with high J_{sc} (Wu et al., 2001a)

Cell #	V_{oc} (mV)	J_{sc} (mA/cm^2)	FF (%)	Efficiency (%)	Area (cm^2)
1	847.5	25.86	74.45	16.4	1.131
2	845.0	25.88	75.51	16.5	1.032

Table 5
J_{sc} losses in a 16.1%-efficient CTO/ZTO/CdS/CdTe solar cell

	J_{sc} loss mechanism	J (mA/cm^2)	$J/J_{theoretical}$ (%)
J_1	Absorption of CTO/ZTO	0.74	2.51
J_2	Absorption of CdS	1.40	4.75
J_3	Recombination in junction and CdTe	0.52	1.76
J_4	Reflection	1.19	4.03
J_{loss}	$J_1 + J_2 + J_3 + J_4$	3.85	13.05
J_{sc}		25.65	86.95
$J_{theoretical}$ $E_g \sim 1.48$ eV		29.5	100

TCO film with high conductivity, and integrating a ZTO buffer layer to optimize $CdCl_2$ treatment for improving junction quality. The increase of R_{sh} is mainly due to integrating a ZTO buffer layer, which reduces the probability of forming localized TCO/CdTe junctions when the CdS film is thinned and acts as an etch-stop layer during the back-contact formation process.

3.2. High short-circuit current density

Table 4 lists I–V parameters of two high-efficiency CdTe cells with J_{sc} of nearly 26 mA/cm^2. In this work, high J_{sc}'s were achieved in three ways: reducing J_{sc} loss due to TCO absorption; reducing J_{sc} loss due to CdS absorption; and reducing J_{sc} loss due to recombination in the junction and CdTe regions. Table 5 lists four different J_{sc} losses in a 16.1%-efficient CTO/ZTO/CdS/CdTe cell (V_{oc} = 842.2 mV, J_{sc} = 25.65 mA/cm^2, and FF = 74.67%), which can be calculated from AM1.5 global solar spectrum, the absolute internal quantum efficiency of this cell, and independent reflection and absorption measurements of individual layers (including glass substrate, CTO, ZTO, and CdS) (Sites, 2003).

It can be seen from Table 5 that (1) the J_{sc} loss due to glass/CTO/ZTO absorption is reduced to 0.74 mA/cm^2, because both the CTO TCO film and the ZTO buffer layer have high transmission and near-zero absorbance in the active wavelength region (400–860 nm); (2) the J_{sc} loss due to CdS absorption is reduced to 1.4 mA/cm^2, because a thinner CdS film (~700–800 nm) can be used, and CdS can be "consumed" partially during the CdTe deposition and $CdCl_2$ treatment processes by integrating a ZTO buffer layer; (3) the J_{sc} loss due to recombination in the junction and CdTe regions is reduced to 0.52 mA/cm^2, because the $CdCl_2$ treatment has been optimized to improve junction and CdTe film quality by integrating a ZTO buffer layer.

3.3. High-efficiency CTO/ZTO/CdS/CdTe cells

A number of CTO/ZTO/CdS/CdTe cells with NREL-confirmed efficiencies of more than 15.8% have been

Table 6
High-efficiency CTO/ZTO/CdS/CdTe solar cells (Wu et al., 2001a)

Cell #	V_{oc} (mV)	J_{sc} (mA/cm^2)	FF (%)	Efficiency (%)	Area (cm^2)
1	844.0	25.21	74.41	15.9	1.004
2	848.2	25.55	73.55	15.9	1.040
3	846.3	25.43	74.24	16.0	1.130
4	849.9	25.50	74.07	16.1	1.029
5	835.6	25.25	76.52	16.1	0.961
6	842.2	25.65	74.67	16.1	0.948
7	842.7	25.24	76.04	16.2	1.116
8	847.5	25.86	74.45	16.4	1.131
9	845.0	25.88	75.51	16.5	1.032

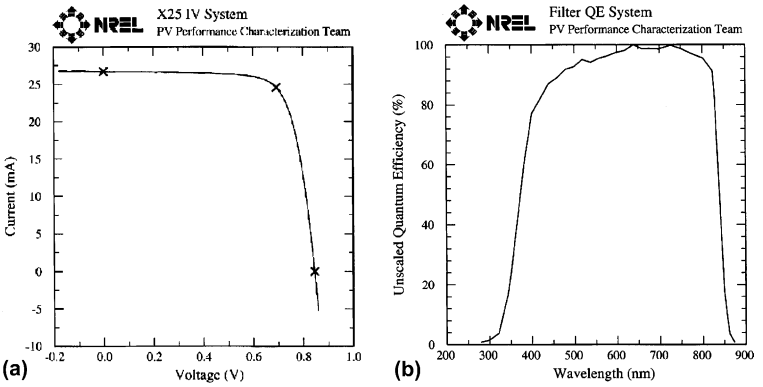

Fig. 11. Current–voltage (a) and relative quantum efficiency (b) curves for 16.5%-efficient CdS/CdTe polycrystalline thin-film solar cell.

fabricated (see Table 6). These results also indicate that the modified CTO/ZTO/CdS/CdTe device structure provides better reproducibility.

In Fig. 11(a), we show a CTO/ZTO/CdS/CdTe polycrystalline thin-film solar cell with an NREL-confirmed total-area efficiency of 16.5% (V_{oc} = 845.0 mV, J_{sc} = 25.88 mA/cm^2, FF = 75.51%, and area = 1.032 cm^2). We believe that this is the highest efficiency ever reported for a CdTe-based solar cell. Fig. 11(b) shows the relative quantum efficiency curve for this cell.

3.4. Future work

The best photovoltaic parameters achieved in our work are V_{oc} = 858 mV (only ~58% of the CdTe bandgap E_g of ~1.48 eV for NREL CdTe film), J_{sc} = 25.9 mA/cm^2 (~87.7% of the theoretical maximum J_{sc} of 29.5 mA/cm^2), and FF = 77.3%. In the short term, a conversion efficiency of 17–18% can be expected by optimizing the device J_{sc} to ~90% of theoretical and the FF to 78–80%. To achieve CdTe cells with an efficiency of 18–20%, research should focus on improving the ratio of V_{oc}/E_g to at least 60% (V_{oc} ~ 900 mV). This could be achieved in three ways: (1) improve the built-in potential by minimizing compensation and increasing doping of the CdTe film; (2) improve the diode quality factor A by minimizing the recombination-center density in the junction region; and (3) reduce the back-contact barrier height.

4. Novel manufacturing processes

Commercial-scale CdTe modules with efficiencies of 6–8% were produced by several CdTe deposition techniques, and they have demonstrated the ability to attract production-scale capital investments. However, there are undesirable issues in the conventional CdTe module manufacturing processes. First, further improvement on performance and yield of CdTe modules have been limited by use of the conventional SnO_2/poly-CdS/poly-CdTe device structure. For example, a thicker CdS layer has to be used for maintaining high yield, which also results in low J_{sc} and low efficiency. Second, the conventional processes include time-consuming and expensive heat-up and cool-down segments that limit throughput and yield, and some "wet" processes that generate a large amount of liquid waste.

To apply our high-efficiency CdTe cell fabrication technique, we developed two manufacturing processes for minimizing these issues and producing high-efficiency CdTe modules.

(1) Process #1 (Wu and Sheldon, 2000b). Fig. 12(a) shows a schematic representation of this novel process. Compared to conventional manufacturing processes, there are several new aspects in this process. First, a borosilicate glass/CTO/ZTO/nano-CdS:O/CdTe device structure was used (see Fig. 12(b)) in this process, which is similar to that used in a high-efficiency CdTe cell. This means that much knowledge on novel materials and the modified device structure can easily transfer to a manufacturing process. Second, the first three layers (including CTO TCO layer, ZTO buffer layer, and CdS:O window layer) are prepared by the same deposition technique—RF magnetron sputtering at room temperature. RF sputtering is a mature technology with demonstrated production scalability. Third, the new process has only one heat-up segment in the entire device fabrication process. The recrystallization of the first three layers and the interdiffusion at the three interfaces (including the CTO/ZTO, ZTO/CdS, and CdS/CdTe interfaces) are completed during CdTe deposition by the CSS technique.

We have fabricated a CTO/ZTO/nano-CdS:O/CdTe cell with an NREL-confirmed efficiency of 14.7% (V_{oc} = 833.8 mV, J_{sc} = 24.06 mA/cm^2, FF = 73.29%,

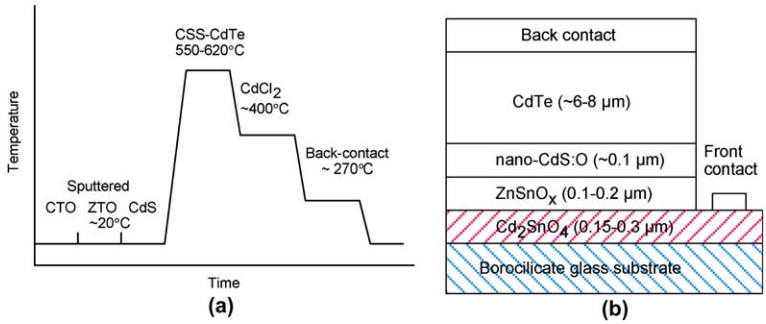

Fig. 12. (a) Schematic representation of novel manufacturing process #1, and (b) a borosilicate glass/CTO/ZTO/nano-CdS:O/CdTe device structure used in process #1.

and area = 1.159 cm^2) by this process. This result is not optimized yet. The device results also demonstrate that CdTe cells prepared by this process have good uniformity, which is desirable for scaling up the process and helping reduce the efficiency gap between small-area cells and modules.

(2) Process #2 (Wu and Zhou, 2004). This process can fabricate high-efficiency CdTe cells on low-cost commercial SnO_2/soda-lime (SL) glass substrates. Fig. 13(a) and (b) show a schematic representation of process #2 and the device structure used in this process, respectively. Soda-lime glass has poorer properties than borosilicate glass, such as higher thermal expansion coefficient, higher Na and Fe content, higher absorbance, and lower softening temperature. Commercial SnO_2 TCO films have an inherent sheet resistivity of $\sim$10−15 Ω/sq and an average transmission of $\sim$80%, which is not good enough to improve CdTe cell performance. However, commercial SnO_2/SL-glass substrates are inexpensive, which is helpful for reducing the CdTe module cost. In this process, performance and reproducibility of CdTe cells were improved significantly by integrating a ZTO buffer layer. The J_{sc} values of CdTe cells were also improved greatly by using nano-CdS:O film. Both the ZTO film and the CdS:O film are prepared by RF magnetron sputtering at room temperature. The entire process contains only one heat-up segment. When using commercial SnO_2/SL-glass substrates with a lower softening temperature, CdTe deposition must be performed at temperatures below 570 °C. The effects of lowering the CdTe deposition temperature impact structural properties and density of the CdTe films. The CdTe film can be deposited by CSS or vapor transport deposition (VTD). We have optimized the deposition parameters in CSS process, such as the source and substrate temperature, total pressure, and partial O_2 pressure, to obtain high-quality and denser CdTe films. We have fabricated a number of CdTe cells on commercial Tek 15 SnO_2/SL-glass (produced by LOF) with NREL-confirmed efficiencies of more than 14%. The best cell has an efficiency of 14.4% (V_{oc} = 829.3 mV, J_{sc} = 23.48 mA/cm^2, and FF = 74.07%). This process also demonstrated better uniformity, which can help to reduce the efficiency gap between small-area cells and modules.

These two novel manufacturing processes provide attractive alternatives for producing CdTe modules with a potential of high throughput and low cost by (1) increasing device efficiency, (2) improving device yield, and (3) simplifying the device fabrication process.

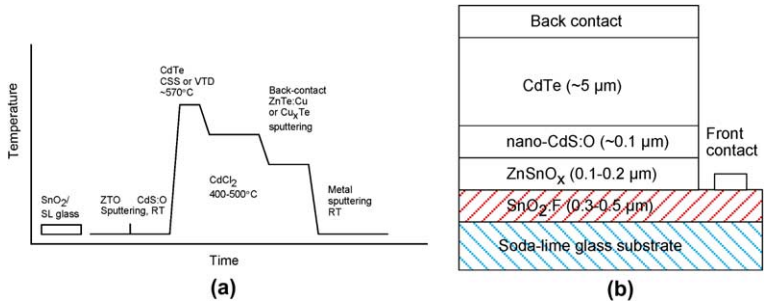

Fig. 13. (a) Schematic representation of novel manufacturing process #2, and (b) a soda-lime glass/SnO_2/ZTO/nano-CdS:O/CdTe device structure used in process #2.

5. Conclusions

Three novel materials (CTO TCO film, ZTO buffer layer, and nano-CdS:O window layer) and a modified CTO/ZTO/CdS/CdTe device structure were developed to minimize some issues related to conventional SnO_2/CdS/CdTe cells, and to further improve performance and reproducibility of CdTe cells. Cd_2SnO_4 transparent conductive oxide films have several significant advantages over conventional SnO_2 TCO films. They have higher conductivity, higher transmission, and near-zero absorption in the active wavelength region. Replacing the SnO_2 TCO film with a Cd_2SnO_4 film can improve J_{sc} and FF of CdTe cells. $ZnSnO_x$ films have several excellent properties, such as high bandgap, high transmittance, and low absorbance, and they can act as a buffer layer between the TCO and CdS layers in CdTe cells. Of special note, there is beneficial interdiffusion between the ZTO and CdS layers, which occurs either at higher temperature (550–650 °C) in Ar or at lower temperature (400–420 °C) in $CdCl_2$ atmosphere. This feature can be used to improve device performance and reproducibility. An oxygenated nanocrystalline CdS:O window layer has a higher optical bandgap (2.5–3.1 eV) than the poly-CdS film; the bandgap increases with an increase of oxygen content and a decrease of grain size. The higher oxygen content presented in the nanocrystalline CdS:O films can significantly suppress the Te diffusion from the CdTe into the CdS film and the formation of a $CdS_{1-y}Te_y$ alloy with a lower bandgap that results in poor quantum efficiency in the short-wavelength region. A CTO/ZTO/CdS/CdTe polycrystalline thin-film solar cell with an NREL-confirmed total-area efficiency of 16.5% (V_{oc} = 845.0 mV, J_{sc} = 25.88 mA/cm^2, FF = 75.51%, and area = 1.032 cm^2) was achieved, which is the highest efficiency ever reported for CdS/CdTe solar cells. To apply the high-efficiency CdTe cell fabrication technique, two novel manufacturing processes for producing high-efficiency CdTe modules were developed. CdTe cells with NREL-confirmed total-area efficiencies of more than 14% were produced using these manufacturing processes.

Acknowledgment

The author would like to thank his colleagues: R.G. Dhere, D.S. Albin, J. Zhou, J.C. Keane, C. DeHart, A. Duda, X. Li, T.A. Gessert, Y. Yan, S. Asher, C. Perkins, G. Teeter, D.H. Levi, M.J. Romero, H.R. Moutinho, B. To, K. Emery, T. Moriarty, and D. Dunlavy for their great contributions to this work; and managers: L. Kazmerski, J. Benner, P. Sheldon, T.J. Coutts, K. Zweibel, and R. Noufi for their encouragement and support. This work is supported by the U.S. Department of Energy under Contract No. DE-AC36-99GO10337 to NREL.

References

Adirovich, E.I., Yuabov, Yu.M., Yagudaev, G.R., 1969. Photoelectric effects in film diodes with CdS–CdTe heterojunctions. Sov. Phys. Semicond. 3, 61–65.

Britt, J., Ferekides, C., 1993. Thin-film CdS/CdTe solar cell with 15.8% efficiency. Appl. Phys. Lett. 62 (22), 2851–2852.

Chu, T.L., Chu, S.S., Schultz, N., Wang, C., Wu, C.Q., 1992. Solution-grown CdS films for photovoltaic devices. J. Electrochem. Soc. 139 (9), 2443–2446.

Chu, T.L., Chu, S.S., 1993. Recent progress in thin-film cadmium telluride solar cells. Prog. Photovoltaics: Res. Appl. 1, 31–42.

Coutts, T.J., Wu, X., Mulligan, W.P., Webb, J.M., 1996. High-performance, transparent conducting oxides based on cadmium stannate. J. Electron. Mater. 25 (6), 935–943.

McCandess, B.E., Hegedus, S.S., 1991. Influence of CdS window layer on thin-film CdS/CdTe solar cell performance. In: Proceedings of 22nd IEEE PVSC, pp. 967–972.

Moutinho, H.R., Dhere, R.G., Al-Jassim, M.M., Ballif, C., Levi, D.H., Swartzlander, A.B., Yong, M.R., Kazmerski, L.L., 2000. Study of CdTe/Cds solar cells using CSS CdTe deposited at low temperature. In: Proceedings of 20th IEEE PVSC, pp. 646–649.

Ohata, K., Saraie, J., Tanaka, T., 1973. Phase diagram of the CdS–CdTe pseudobinary system. Jpn. J. Appl. Phys. 12 (10), 1198–1204.

Ohyama, H., Aramoto, T., Kumazawa, S., Higuchi, H., Arita, T., Shibutani, S., Nishio, T., Nakajima, J., Tsuji, M., Hanafusa, A., Hibino, T., Omura, K., Murozono, M., 1997. 16.0%-efficient thin-film CdS/CdTe solar cells. In: Proceedings of 26th IEEE PVSC, pp. 343–346.

Sites, J.R., 2003. Quantification of losses in thin-film polycrystalline solar cells. Sol. Energ. Mat. Sol. C. 75, 243–251.

Ullal, H.S., Zweibel, K., von Roedern, B.G., 2000. Polycrystalline thin-film photovoltaic technologies: from laboratory to commercialization. In: Proceedings of 28th IEEE PVSC, pp. 418–424.

Wei, S., Zhang, S.B., Zunger, A., 2000. First-principles calculation of band offsets, optical bowings, and defects in CdS, CdSe, CdTe, and their alloys. J. Appl. Phys. 87 (3), 1304–1311.

Wu, X., Mulligan, W.P., Coutts, T.J., 1996a. Recent developments in RF sputtered cadmium stannate films. Thin Solid Films 286, 274–276.

Wu, X., Sheldon, P., Coutts,T.J., Rose, D.H., Mulligan, W.P., Moutinho, H.R., 1996b. CdS/CdTe thin-film devices using a Cd_2SnO_4 transparent conductive oxide. In: Proceedings of 14th NREL/SNL PV Program Review Meeting, pp. 693–702.

Wu, X., Sheldon, P., Coutts, T.J., Rose, D.H., Moutinho, H.R., 1997. Application of Cd_2SnO_4 transparent conductive oxides in CdS/CdTe thin-film devices. In: Proceedings of 26th IEEE PVSC, pp. 347–350.

Wu, X., Sheldon, P., Mahathongdy, Y., Ribelin, R., Mason, A., Moutinho, H.R., Coutts, T.J., 1998. CdS/CdTe thin-film solar cell with a zinc stannate buffer layer. In: Proceedings of 15th NREL/SNL PV Program Review Meeting, pp. 37–41.

Wu, X., Ribelin, R., Dhere, R.G., Albin, D.S., Gessert, T.A., Asher, S., Levi, D.H., Mason, A., Moutinho, H.R., Sheldon, P., 2000. High-efficiency Cd_2SnO_4/Zn_2SnO_4/

$Zn_xCd_{1-x}S$/CdS/CdTe polycrystalline thin-film solar cells. In: Proceedings of 28th IEEE PVSC, pp. 470–474.

Wu, X., Sheldon, P., 2000. A novel manufacturing process for fabricating CdS/CdTe polycrystalline thin-film solar cells. In: Proceedings of 16th European PVSEC, pp. 341–344.

Wu, X., Keane, J.C., Dhere, R.G., DeHart, C., Albin, D.S., Duda, A., Gessert, T.A., Asher, S., Levi, D.H., Sheldon, P., 2001a. 16.5%-efficient CdS/CdTe polycrystalline thin-film solar cells. In: Proceedings of 17th European PVSEC, pp. 995–1000.

Wu, X., Asher, S., Levi, D.H., King, D.E., Yan, Y., Gessert, P., Sheldon, P., 2001b. Interdiffusion of CdS and Zn_2SnO_4 layers and its application in CdS/CdTe polycrystalline thin-film solar cells. J. Appl. Phys. 89 (8), 4564–4569.

Wu, X., Dhere, R.G., Yan, Y., Romero, M.J., Zhang, Y., Zhou, J., DeHart, C., Duda, A., Perkins, C., To, B., 2002. High-efficiency polycrystalline CdTe thin-film solar cells with an oxygenated amorphous CdS (a-CdS:O) window layer. In: Proceedings of 29th IEEE PVSC, pp. 531–535.

Wu, X., Dhere, R.G., Zhou, J., Duda, A., Perkins, C., Yan, Y., Moutinho, H.R., 2003. High-quality cadmium stannate transparent conductive oxide film for tandem thin-film solar cells. In: Proceedings of Third World PVSEC, pp. 507–510.

Wu, X., Yan, Y., Dhere, R.G., Zhang, Y., Zhou, J., Perkins, C., To, B., 2003b. Nanostructured CdS:O film: preparation, properties, and application. Phys. Stat. Sol., 1062–1066.

Wu, X., Zhou, J., 2004. High-efficiency CdTe solar cells on commercial SnO_2/soda-lime glass prepared by novel manufacturing process. In: Proceedings of 19th European PVSEC, in press.